LOW ORDER MODELING OF HIGH FREQUENCY COMBUSTION INSTABILITIES IN LIQUID ROCKET ENGINES

Alexandre Fougnie, Schmitt Thomas, Sebastien Ducruix

SP2020_00043

LOW ORDER MODELING OF HIGH FREQUENCY COMBUSTION INSTABILITIES IN LIQUID ROCKET ENGINES

Alexandre Fougnie[(1),(2)], Thomas Schmitt[(1)], Sébastien Ducruix[(1)]

[(1)] Laboratoire EM2C, CNRS, CentraleSupélec, Université Paris-Saclay, Bâtiment Eiffel, 3 rue Joliot Curie, 91192 Gif-sur-Yvette, France
alexandre.fougnie@centralesupelec.fr
thomas.schmitt@centralesupelec.fr
sebastien.ducruix@centralesupelec.fr

[(2)] CNES, Launchers Directorate, 52 Rue Jacques Hillairet, 75612 Paris Cedex, France

KEYWORDS:

liquid rocket propulsion, thermo-acoustic instabilities, high-frequency instabilities, low order modeling, transverse acoustic response, Galerkin modal expansion

ABSTRACT:

Using a Galerkin modal expansion, a low-order modeling approach allows to predict pressure variations resulting from high-frequency combustion instabilities within the liquid rocket propulsion framework. By projecting the pressure oscillations over the engine's eigenmodes base, a decoupling of temporal and spatial aspects simplifies the acoustic equation resolution. Source terms in the differential equation account for phenomena such as the combustion response to acoustic solicitations. Models for combustion, injection dynamics, and external excitation are given. The possibility to track acoustic energy and acoustic power balance provides a finer analysis of the results. The tool capacities and robustness are demonstrated through 2-dimensional open and closed duct computation related to an analytical stability study, and comparisons with an experimental test rig and large eddy simulation (LES) results.

1. INTRODUCTION

High-frequency combustion instabilities constitute a significant hindrance for liquid rocket engine (LRE) development since the beginning of the space age, see [1, 2]. Within an LRE, seen as a confined environment, an intricate coupling between the flames combustion response, the acoustic, and the injection dynamics can lead to tremendous pressure oscillations compromising the engine's integrity. When the combustion noise excites a specific engine's eigenmode, mostly the transverse modes, which are of high frequency, acoustic pressure and velocity variations disturb the flow at injection and flames unsteady heat release, generating more acoustic perturbations that feed the instabilities [3]. The principal prediction tools are experimental tests, computational fluid dynamics calculations such as large-eddy simulation (LES) and low order modeling giving the acoustic modes shape with their tendency to be unstable.

When instabilities are encountered during development or qualification campaigns, many additional tests are necessary, changing the injection units geometry, adding baffles and rods, to change the mode's structures and shift the natural frequencies, as reviewed in [4]. Therefore, the process is expensive and prolonged. Still, the experiments at laboratory-scale make it possible to observe the flame structure close to real operating conditions, see [5], and their response to transverse solicitations, see [6–9]. Moreover, the study of the resonance between the combustion chamber and the injection system [10–12] has shown that the central phenomenon responsible for the unsteady heat release variations are the propellant injection velocity oscillations and not the transverse acoustic disturbance directly on the flame.

These observations are supplemented by numerical studies allowing better targeting of the phenomena at stake. LES computations show the annular jet structures of injected propellants under transverse acoustic forcing [13,14], in middle-scale combustion chamber [15, 16] giving access to the influence of acoustic, vorticity and entropy terms, and non-linear modes coupling.

Although these are very information-rich ap-

proaches to understand the phenomena involved, these tools are ill-suited for engine design loops. Thus, low-order modeling strategies have emerged in recent years, aiming to reduce the need for long and costful hot-fire tests and CFD computations.
Solving Helmholtz's equation, the acoustic equation in the frequency domain, gives access to the engine's resonant modes, using finite element resolution and fixed-point iteration. However, for real cases, to find all the relevant modes can become complex, and the algorithm convergence is not ensured, see [17]. Using Riemann invariants for acoustic network reduces computational time considerably, see [18], but study cases are limited to longitudinal acoustic networks. Galerkin expansion methods enable, by projecting the pressure variations onto the modes, to keep the geometry complexity, working on transverse and longitudinal coupled modes [19]. Hybrid Galerkin-Riemann solvers have the same abilities, using Riemann invariants to tackle longitudinal components and Galerkin expansion for transverse ones. Besides, the engine's geometry can be decomposed into acoustic elements characterized by acoustic equations specific to each element and assembled using precise boundary conditions, as in the state-space approach [17], or handled in is whole [20]. This paper first present the low order tool developed using modal expansion on Sec.2. Combustion modeling is discussed Sec.3 and an open-tube with a flame validation case is performed Sec.4. Then, Sec.5 underlines the ability to model and reproduce experimental data. Finally, a discussion and conclusion are proposed Sec.6.

2. LOW ORDER MODELING

The purpose of low order modeling is to provide a simplified framework for thermo-acoustic instabilities, using models to describe the driving and damping mechanisms. Although the prediction accuracy is limited by one's capacity to translate phenomena that intervene in the instabilities into workable modelings, the computational cost needed to solve the given framework are less demanding than those needed to solve an LES computation.

2.1. Galerkin expansion

The presented hereafter approach is based on a Galerkin expansion of the pressure variations p' over the base formed by the engine's eigenmodes, such that:

$$p'(\mathbf{x},t) = \sum_{n=1}^{\infty} \eta_n(t)\Psi_n(\mathbf{x}) \qquad \text{Eq.1}$$

where η_n represents the temporal evolution of the n$^{\text{th}}$ mode and Ψ_n its spatial structure, $(\Psi_n)_{n\geq 1}$ being a base on which one can project any pressure signal obtain. This decomposition was first proposed by [19] and developed by [21,22], then recently studied in [17,23]. The main advantage is that the temporal aspect can be detached from the spatial structure while handling complex geometries, with longitudinal, transverse, and coupled modes, where methods based on Riemann invariants, for example, are limited to acoustic networks with longitudinal wave propagation. This projection on the base $(\Psi_n)_{n\geq 1}$ constitutes the central element of the method and allows to simplify the equations describing the physics of the engine. By using this projection in the acoustic equation, the partial differential equation (PDE) on the pressure is reduced to a set of ordinary differential equations (ODE) for each mode, easier to solve numerically. Then, still keeping this decomposition as a central element, models are provided to these equations as a source term to account for desired phenomena. The main difficulty is to translate physical behaviors into this particular form of modeling. This method offers modularity and attractive ease of adaptation for industrial needs.

To obtain the framework used to predict thermo-acoustic instabilities, let's consider the conservation equations of mass Eq.2, momentum Eq.3, energy Eq.4 and the perfect gas equation of state Eq.5

$$\frac{\partial \rho}{\partial t} + \nabla.\rho\mathbf{u} = 0 \qquad \text{Eq.2}$$

$$\rho\left(\frac{\partial \mathbf{u}}{\partial t} + \mathbf{u}.\nabla\mathbf{u}\right) = -\nabla p \qquad \text{Eq.3}$$

$$\rho T\left(\frac{\partial s}{\partial t} + \mathbf{u}.\nabla s\right) = \dot{q} \qquad \text{Eq.4}$$

$$p = \rho^{\gamma} e^{s/c_v} \qquad \text{Eq.5}$$

with ρ the density, $\mathbf{u} = (u_1, u_2, u_3)$ the velocity vector, p the pressure, T the temperature, s the entropy of the flow, $\dot{q}$ the heat release per unit volume, γ the specific heat ratio and c_v the specific heat of the mixture at constant volume. Using linearization such that each value x is decomposed as a constant component $\bar{x}$ and a first order variation x' such that $x = \bar{x} + x'$, and a zero Mach number hypothesis stating $\bar{u}$ as a first order term, Eqs.2-5 gives the following formulation Eq.6 for the acoustic equation, keeping first order terms:

$$\frac{\partial^2 p'(\mathbf{x},t)}{\partial t^2} - \gamma\bar{p}\nabla.(\frac{1}{\bar{\rho}}\nabla p'(\mathbf{x},t)) = (\gamma-1)\frac{\partial \dot{q}'}{\partial t} \qquad \text{Eq.6}$$

The zero Mach number assumption simplifies the set of equations, but is a quite strong hypothesis since not valid in full-size rocket engine where the mean value of the velocity $\bar{\mathbf{u}}$ can not be considered of first order. However, this formulation produces satisfactory results for lab-scale experiments and theoretical-analytical comparison.

Remembering Eq.1, $(\eta_n)_{n>1}$ and $(\Psi_n)_{n\geq 1}$ are needed in order to reconstruct the pressure variations. On one hand, by using harmonic perturbations for the quantities and passing in the frequency domain, Eq.6 gives the Helmholtz equation

Eq.7 [24], verified for each mode, with no combustion response, where $\omega_m = 2\pi f_m$ is the pulsation of the m[th] mode and f_m its eigenfrequency.

$$\gamma\bar{p}\nabla.\left(\frac{1}{\bar{\rho}}\nabla\Psi_m\right) + \omega_n^2\Psi_m = 0 \qquad \text{Eq.7}$$

Two assumptions are then made. First, a finite number of modes N is considered, so there is a truncation of the sum in Eq.1. Second, homogeneous Neumann or Dirichlet boundary conditions are considered in order to solve in the Helmholtz solver the Eq.7, so $\nabla\Psi_m(\mathbf{x}_s).\mathbf{n} = 0$ and $\Psi_m(\mathbf{x}_s) = 0$ with $\mathbf{x}_s$ located on the boundaries of the geometry. In other words, boundary conditions of Neumann where the acoustic speed $\mathbf{u}'(\mathbf{x}_s, t).\mathbf{n} = 0$ or of Dirichlet such as $p'(\mathbf{x}_s, t) = 0$ are imposed. Thus, the Helmholtz equation resolution gives the eigenfrequencies and eigenmodes of the geometry, and the obtained modal base $(\Psi_n)_{N\geq n\geq 1}$ is orthogonal, with $\Lambda_n\delta_{nm} = \int_V \Psi_n\Psi_m dV$ the square L^2 norm so that $\Lambda_n = \int_V \Psi_n^2 dV$.

The last unknows to access pressure are the $(\eta_n)_{n\geq 1}$ and their determination is the main goal of the low order approach proposed.

2.2. Modal amplitude differential equation

By combining Eq.6$*\Psi_m$ and Eq.7$*p'$:

$$\begin{aligned}&\frac{\partial^2 p'}{\partial t^2}\Psi_m + \omega_n^2\Psi_m p' + \gamma\bar{p}\nabla.\left(\frac{1}{\bar{\rho}}\nabla\Psi_m\right)p' \\ &- \gamma\bar{p}\nabla.\left(\frac{1}{\bar{\rho}}\nabla p'\right)\Psi_m = (\gamma-1)\frac{\partial\dot{q}'}{\partial t}\Psi_m\end{aligned} \qquad \text{Eq.8}$$

Then an integration of Eq.8 over the volume V of the domain and the use of the projection Eq.1 give:

$$\begin{aligned}&\sum_{n=1}^{N}\ddot{\eta}_n(t)\int_V \Psi_n\Psi_m dV + \omega_m^2\sum_{n=1}^{N}\eta_n(t)\int_V \Psi_n\Psi_m dV \\ &+ \int_V \gamma\bar{p}\left(p'\nabla.\left(\frac{1}{\bar{\rho}}\nabla\Psi_m\right) - \Psi_m\nabla.\left(\frac{1}{\bar{\rho}}\nabla p'\right)\right)dV \\ &= (\gamma-1)\int_V \frac{\partial\dot{q}'}{\partial t}\Psi_m dV\end{aligned} \qquad \text{Eq.9}$$

Using the orthogonality property, and Green identity on the third volume integral, Eq.9 is projected onto each mode, so that a set of N differential equations is obtained, for each m mode:

$$\begin{aligned}&\ddot{\eta}_m(t) + \omega_m^2\eta_m(t) + \frac{1}{\Lambda_m}\int_S c_0^2 p'\nabla\Psi_m.n \\ &- c_0^2\Psi_m\nabla p'.ndS = \frac{\gamma-1}{\Lambda_m}\int_V \frac{\partial\dot{q}'}{\partial t}\Psi_m dV\end{aligned} \qquad \text{Eq.10}$$

The imposed boundary conditions allow the surface integral simplification, thus, for all $N \geq m \geq 1$:

$$\ddot{\eta}_m(t) + \omega_m^2\eta_m(t) = \frac{\gamma-1}{\Lambda_m}\int_V \frac{\partial\dot{q}'}{\partial t}\Psi_m dV \qquad \text{Eq.11}$$

The right hand side term is the combustion source term, where a formulation for $\dot{q}'$ has to be given. The idea is to model as source term any physical process one may want to account for. By adding terms for the damping $S_{damping}$ and driving $S_{driving}$ aspects, the proposed approach has reduced the acoustic equation into a set of N simpler equations represented by Eq.12 for each m mode.

$$\ddot{\eta}_m(t) + \omega_m^2\eta_m(t) = S^m_{damping} + S^m_{driving} \qquad \text{Eq.12}$$

To solve Eq.12, initial conditions are needed. These conditions are obtained by projecting a given initial pressure $p'(\mathbf{x}, t_0)$ and $\dot{p}'(\mathbf{x}, t_0)$ fields into the modal base:

$$\eta_m(0) = \frac{1}{\Lambda_m}\int_V p'(\mathbf{x}, t_0)\Psi_m(\mathbf{x})dV \qquad \text{Eq.13a}$$

$$\dot{\eta}_m(0) = \frac{1}{\Lambda_m}\int_V \dot{p}'(\mathbf{x}, t_0)\Psi_m(\mathbf{x})dV \qquad \text{Eq.13b}$$

2.3. Acoustic energy balance

The modal decomposition allows accessing the variations of acoustic pressure within the geometry of interest. It is possible to go further in the characterization of instabilities, mainly if one thinks of the Rayleigh criterion [25], by analyzing the energies and powers at stake. Thus the acoustic energy E_a can be tracked using:

$$E_a(x,t) = \frac{1}{2}\frac{p'^2}{\bar{\rho}\bar{c}^2} + \frac{1}{2}\bar{\rho}\mathbf{u}'^2 \qquad \text{Eq.14}$$

with the acoustic velocity field being

$$\mathbf{u}' = -\frac{1}{\bar{\rho}}\sum_{n=1}^{N}\int_t \eta_n(t)dt\nabla\Psi_n(\mathbf{x}) \qquad \text{Eq.15}$$

Moreover, the acoustic balance [25] represented by Eq.16 offers the possibility to observe the temporal evolution of each phenomena contribution to the instabilities. Speaking of combustion, when the Rayleigh power term R_a is positive, then the combustion feeds the instabilities and flames that act like a driving system, however, when R_a is negative, then flames act as a damping device.

$$\frac{\partial E_a}{\partial t} + \text{Flux} = R_a + D \qquad \text{Eq.16}$$

with the acoustic power

$$\frac{\partial Ea}{\partial t} = \frac{\dot{p}'p'}{\bar{\rho}\bar{c}^2} + \bar{\rho}\dot{\mathbf{u}}'.\mathbf{u}' \qquad \text{Eq.17}$$

the Rayleigh power

$$R_a = \frac{\gamma-1}{\gamma\bar{p}}p'\dot{q}' \qquad \text{Eq.18}$$

and the flux at boundaries

$$\text{Flux} = \int_V \nabla.p'\mathbf{u}'dV = \oint_S p'\mathbf{u}'.ndS \qquad \text{Eq.19}$$

Subsequently, for any source term models made, it is necessary to develop the associated power to use this energetic approach. Moreover, the damping power formulation for the D term of Eq.16 is not explained here because the associated source term for damping effects has not yet been discussed in the paper.

2.4. Discussion

Assumptions have been made, quite reductive of the LRE conditions, such as the low Mach number and the perfect gas assumption. Moreover, the modal base obtained possesses homogeneous boundary conditions, limiting the analysis to geometries where Dirichlet or Neumann conditions are imposed. Considering an impedance over a specific portion of the boundaries breaks the mode's orthogonality. As discussed in [22, 23], this issue can be handled to consider, in the case of a rocket engine, an impedance modeling a reflection at nozzle throat.
Therefore, this approach's modularity lies in adding and removing sources terms accounting for combustion, damping, external excitation, and boundary conditions influence, where the modal base incorporates the geometry complexity.

2.5. Low order tool

On this basis, the low order tool StaHF - Stability High Frequency, is under development at the EM2C laboratory. Modeling of combustion, injection dynamics and external excitation were derived using experimental and LES data.

3. COMBUSTION MODELING

Some combustion models have been provided to account for flame response to transverse solicitations. The Flame Acoustic Motion Equations (FAME), proposed by [26], describes the oscillations of a group of fixed length, infinitely thin flames around the mean position characterized by the injection units outlet, under transverse acoustic velocity perturbation, in a parallelepiped combustion chamber. The Spray Dynamic Modeling (SDM), also from [26], accounts for the atomization, vaporization and mixing processes along the flames length. The flames are perceived as a group of droplets whose size varies according to a Weber number. Hence the transverse acoustic field has a different impact depending on the diameters of the droplets. Delay associated with momentum relaxation and local heat release rates influenced by droplet spatial density distribution are introduced, accounting for the atomization, vaporization and mixing processes. A representation of the injection dynamics was given by [27], where the acoustic waves in the chamber influence the pressure change through the injection units and hence leading to oscillations of the mass flow rate at the injectors outlet and unsteady heat release.

The Sensitive Time Lag (STL) model, also called the (n,τ) model, was first introduced by [1] has been implemented in the low order tool since it is still the main modeling used to link the heat release and pressure (or velocity) variation. It allows comparisons to theoretical, numerical and experimental results. It supposes that the heat release is proportional to the pressure variation, through the interaction index n, which is similar to the gain of a transfer function, and considered that the propellant injected in the combustion chamber at the instant $t-\tau$, because of the atomization and mixing process, releases the heat at the instant t, τ being the time lag:

$$\dot{q}'(\mathbf{x},t) = n\frac{\bar{q}}{\bar{u}}u'(\mathbf{x},t-\tau) \qquad \text{Eq.20}$$

with $\bar{u}$ the mean velocity at the injection units outlet and $\bar{q}$ the mean heat release per unit volume. It is interesting to have access to this formulation because it allows many comparison and validation of the framework. However, the determination of values for n and τ demands usually to fit experimental or numerical data, or subsequent modelings to be link to physical processes. To be implemented into the framework of interest, Eq.20 has to be derivated with respect of time and projected into the modal base. The associated combustion source term S^m_{comb} is:

$$S^m_{comb}(t) = \frac{\gamma-1}{\Lambda_m}\int_V \frac{\partial\dot{q}'(\mathbf{x},t)}{\partial t}\Psi_m(\mathbf{x})dV \qquad \text{Eq.21}$$

where

$$\frac{\partial\dot{q}'(\mathbf{x},t)}{\partial t} = n\frac{\bar{q}}{\bar{u}}\frac{\partial u'(\mathbf{x},t-\tau)}{\partial t} \qquad \text{Eq.22}$$

and by making use of the linearized momentum equation that state $\frac{\partial \mathbf{u}'}{\partial t} = -\frac{1}{\bar{\rho}}\nabla p'$, and the gradient of Galerkin expansion $\nabla p'(\mathbf{x},t-\tau) = \sum_{n=1}^{N}\eta_n(t-\tau)\nabla\Psi_n(\mathbf{x})$, the combustion source term becomes:

$$S^m_{comb}(t) = -\frac{\gamma-1}{\Lambda_m}* \int_V \frac{n\bar{q}}{\bar{u}\bar{\rho}}\sum_{n=1}^{N}\eta_n(t-\tau)\nabla\Psi_n(\mathbf{x})\Psi_m(\mathbf{x})dV \qquad \text{Eq.23}$$

In Eq.23, n, $\bar{u}$, $\bar{\rho}$ and $\bar{q}$ parameters are kept in the volume integral since they might be non-uniform. This source term is incorporated in Eq.12 and then solved, providing the $(\eta_n)_{n>1}$ to access the pressure variations with Eq.1.

4. MODELING A FLAME IN AN OPEN DUCT - A VALIDATION CASE

The following test case is the open duct with a flame at mid-length from [3], see Fig.1. Using some hypothesis listed hereafter, the authors establish stability domains for the quarter wave, which is the first

longitudinal mode of this geometry. These stability domains give a frame of the τ parameters driving the combustion response that allows a prediction of the rise or damping of the pressure oscillations by the flame. The hypothesis made are:

- STL flame response with $0 < n < 1$;
- boundary conditions are wall on the left side meaning $u'(x = 0) = 0$ and open on the right side meaning $p'(x = l) = 0$;
- the mean Mach flow number is considered small;
- the dissipation is negligible, so no damping;
- the flame length is considered small;
- the sound speed and density are homogeneous, so $c_1 = c_2 = c$ and $\rho_1 = \rho_2 = \rho$.

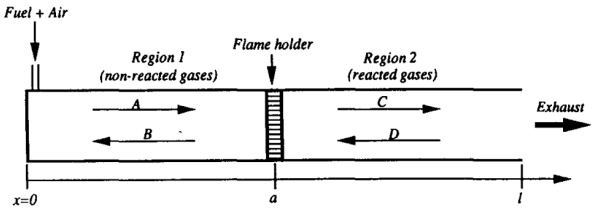

Figure 1: Geometry of the study domain [3]

On this basis, the framing of τ for the quarter wave mode is, with $T_0 = \frac{2\pi}{\omega_0} = \frac{8a}{c}$:

$$-\frac{T_0}{2} + jT_0 < \tau < jT_0 \quad \text{with} \quad j = 1, 2, ... \qquad \text{Eq.24}$$

This means that if the τ is set to a value included in the interval, then the flame introduces energy in the system, leading to an increase of the pressure oscillations and of the acoustic energy. However, if τ is not in these ranges, then the flame acts as a damping device absorbing acoustic energy and reducing the pressure oscillations. Table 1 gives the first intervals of stability for the time lag τ parameter.

j	Stable interval	Instable interval
1	$\frac{T_0}{2} < \tau < T_0$	$T_0 < \tau < \frac{3T_0}{2}$
2	$\frac{3T_0}{2} < \tau < 2T_0$	$2T_0 < \tau < \frac{5T_0}{2}$
3	$\frac{3T_0}{2} < \tau < 3T_0$	$3T_0 < \tau < \frac{7T_0}{2}$

Table 1: Stable and instable intervals for the time lag τ, according to the [3] analysis

Hence, the upper and lower boundary of the ranges are reported into a graph, represented in Fig. 4 by vertical dotted lines. In this graph, the ordinate represents the growth rate g [s^{-1}] of the instability, proposed by [25] as:

$$g = \frac{\mathcal{R}}{2\mathcal{E}} \qquad \text{Eq.25}$$

with

$$\mathcal{E} = \frac{1}{T}\int_T \int_V E_a(\mathbf{x}, t) dV dt \qquad \text{Eq.26}$$

and

$$\mathcal{R} = \frac{1}{T}\int_T \int_V R_a(\mathbf{x}, t) dV dt. \qquad \text{Eq.27}$$

If the growth rate is located in the $g > 0$ area, then this mean that the Rayleigh term integrated over the period and volume $\mathcal{R}$ is positive and that the flame brings energy to the system. This is a zone of instability. On the contrary, when $g < 0$, the Rayleigh term acts as a damping term. This is a zone of stability. Using StaHF code, this problem is solved going through the τ values from 0 to 8ms for a $l = 0.4m$, $c = 435m/s$ and $\rho = 2.58kg/m^3$ domain. Growth rates are computed and reported Fig.4. StaHF results fit well the theoretical values, it reproduces correctly the stability/instability behaviors, with minimum and maximum growth rate values located in the middle of the zones. The τ values found with StaHF that correspond to a $g = 0$ limit stability are compared in term of relative error to the theoretical limits. Error are of the order of 0.1%, and similar results are found for the three-quarter wave stability analysis, in agreement with the theoretical study.

Being able to compute the growth factor g is not the only gain brought by the computation of acoustic energy and powers. It extends the stability analysis since powers variations can be tracked. Figure 2 shows the acoustic power balance for a computation with $\tau = 1.83ms = \frac{T_0}{2}$. In this case, the system is at the stability limit, which can be seen because the Rayleigh power curve is as positive as negative, hence during half a period the flame produce a certain amount of energy and for the second half of the period, the flame damps the same amount of energy.

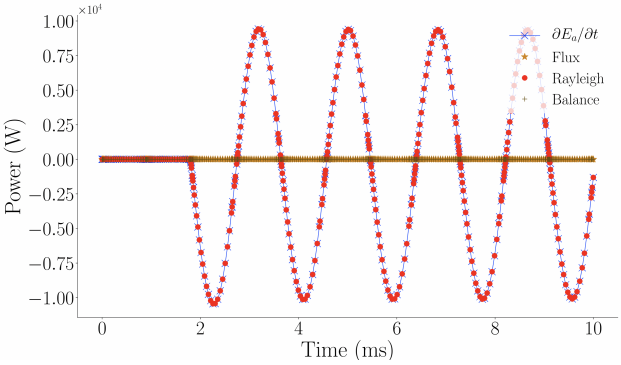

Figure 2: Acoustic balance for a $\tau = 1.83ms$ computation

A curve for an unstable computation such as $\tau = 2.8ms$ (in the first unstable zone as shown in Fig 4), see Fig. 3, shows that the Rayleigh energy is only positive, meaning this configuration is in his most

unstable case that correspond to a maximum on the stability curve Fig. 4 because the pressure wave and heat release are in phase. Similarly, the balance for a computation with $\tau = 1ms$ would show a Rayleigh power only negative, the pressure being in phase opposition with the unsteady heat release.

By tracking the acoustic energy, similar conclusions appear. Although these results are easy to anticipate for this specific simple case, for computation involving several modes and other processes such as damping, the stability analysis is broader thanks to the energetic tool. The last main issue noted is the balance also attest from the quality of the computation since the relation Eq.16 is respected. Both Figs. 2 and 3 show a closed balance.

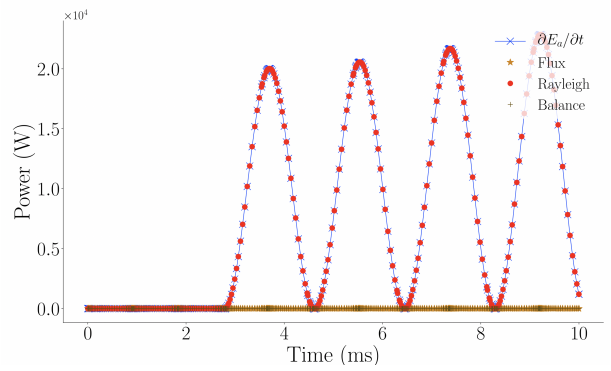

Figure 3: Acoustic balance for a $\tau = 2.8ms$ computation

5. MODELING FORCED TRANSVERSE INSTABILITIES - EXPERIMENTAL COMPARISON

The NPCC test bench, for New Pressurized Coupled Cavities [27], was designed as a cold flow experiment constituted of a dome and a chamber linked by three injection units. It is based on the TPCC test bench, [28], but with the possibility to change the injectors diameter. This results in a change of head losses and affects the chamber/dome coupling. The exhaust chamber that includes two nozzles, upper and lower, and a VHAM (Very High Amplitude Modulation) module, where a rotating toothed wheel closes successively the upper and lower nozzle. This external modulation allows to drive acoustic oscillations within the chamber and to excite targeted eigenmodes. Then it is possible to study how the dome responds to pressure fluctuations in the chamber and so to establish modeling of the injection dynamic. It runs cold flow, meaning air is injected in the dome and goes through the structure, there is no reactive flow and combustion. Figure 5 presents the NPCC geometry. The VHAM has been modeled using the low order framework, in [26], so that the corresponding source term is:

$$S^m_{\text{vham}}(t) = \frac{\dot{m}_{tot}}{2\Lambda_m}\omega_e c^2 \left(\Psi_m(\mathbf{x}_1) - \Psi_m(\mathbf{x}_2)\right)\sin(\omega_e t) \quad \text{Eq.28}$$

where $\dot{m}_{tot}$ is the mass flow rate modulated, ω_e the VHAM excitation frequency, $\Psi_m(\mathbf{x}_1)$ the m^{th} mode evaluated at the upper nozzle position and $\Psi_m(\mathbf{x}_2)$ at the lower nozzle position. The eigenmodes and eigenfrequences need for the StaHF analysis are computed with the Cerfacs Helmholtz solver AVSP [24].

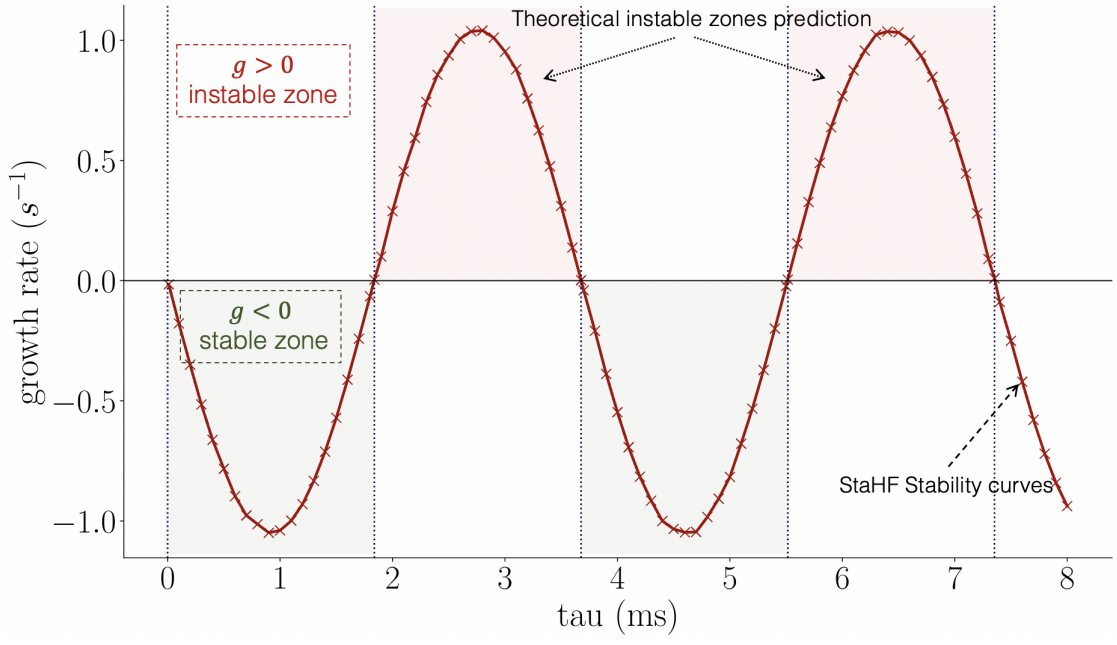

Figure 4: Theoretical stability zones [3] vs Stability curve computed with StaHF for the quarter wave mode. The red zones correspond to the instability domains, since $g > 0$, and the green zones to $g < 0$ stability domains.

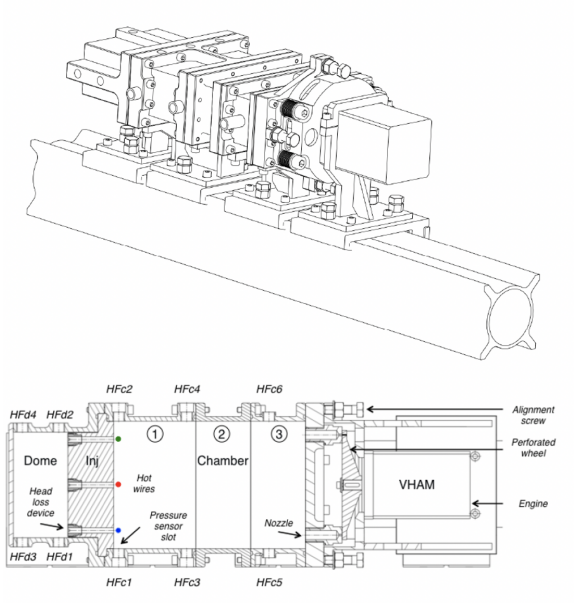

Figure 5: NPCC geometry, constituted from a dome, three injection units and a chamber ended with two nozzles. NPCC is equipped with the VHAM module to close alternatively the upper and lower nozzle, [27]

5.1. Ramp excitation

The first comparison proposed hereafter is a comparison of the pressure response to a VHAM ramp excitation, from 0Hz to 3000Hz on 100s. When the VHAM goes through a frequency corresponding to an acoustic eigenmode of the NPCC, the pressure signal rises because of the resonance phenomenon. Hence, this ramp test is an experimental way of targeting the eigenfrequencies. The modeling parameters, damping coefficient and geometry are entered in the StaHF code, and the obtain ramp pressure signal is compared to the experimental acquisition of [27]. Results are shown Fig. 8 for the experimental response and Fig. 9 for StaHF pressure. So, experimentally, the first longitudinal (1T) mode is found at 1227Hz, the first longitudinal/transverse (1T1L) mode is at 1465Hz, the 1T2L mode is at 2009 Hz and the 1T3L mode at 2686 Hz for the chamber and the first transverse mode for the dome is found at 1487Hz (1TDome). Respectively, the StaHF computation shows simular results, for modes at 1226Hz (1T), 1468Hz (1T1L), 2036Hz (1T2L), 2723Hz (1T3L) and 1485Hz (1TDome), recapitulated in Tab. 2.

Thus StaHF can reproduce this experimental test and activate the eigenmodes of the dome and chamber. Some differences are to be noted, for instance, the 1T3L mode responds much more in the experimental than in the StaHF results. This is due to the lack of precision on the damping coefficient and the mass flow rate modulated, that have been extracted from experimental data in [27]. Are available the approximated coefficients only for the chamber 1T, 1T1L, 1T2L, and 1T3L modes.

	1T	1T1L	1T2L	1T3L	1T-D
Expe	1227	1465	2009	2686	1487
StaHF	1226	1468	2036	2723	1485

Table 2: Experimental frequencies (Hz) of first tangential modes from [27] compared with the StaHF ramp simulation that correspond to the AVSP computed modal frequencies

5.2. Transverse mode excitation in linear domain

The results obtained with StaHF are compared with LES computational results done by D. Marchal, Ph.D. student at the EM2C laboratory. What has been shown using the LES approaches is that, above a certain level of acoustic excitation from VHAM, a nonlinear coupling between modes appears. The excited eigenmode amplitude increases and, reaching a certain threshold, activates a higher order's harmonic modes. Hence the pressure signal that can be measured in the chamber is composed of the fundamental mode but also of the harmonics. However, there is no model to translate this phenomenon in StaHF at this point. Therefore, LES calculations are carried out while remaining in a linear behavior, by lowering the mass flow rate modulated by the VHAM, where only the fundamental mode responds.

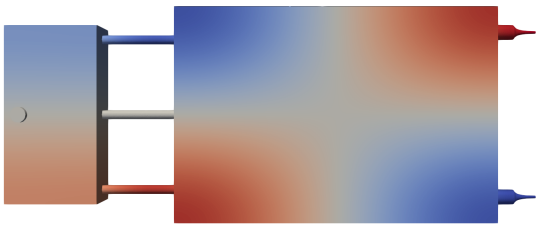

Figure 6: NPCC 1T1L eigenmode computed with AVSP (Cerfacs) [24]

The VHAM is hence set to a frequency of 1468Hz exciting the 1T1L mode, and the modulated mass flow rate is of $5.1 * 10^{-5} kg/s$ and the damping coefficient for this specific mode is $\alpha = 3s^{-1}$, where $S^m_{damping} = 2\alpha\dot{\eta}(t)$. The 1T1L mode computed with the Cerfacs Helmholtz solver AVSP is given Fig. 6. Figure 7 shows the pressure response computed with the LES tool and StaHF. The LES has been run with a frequency of excitation from the VHAM of 1468 Hz. However, it does not correspond to the mode's exact frequency since the AVSP modal calculation made does not account for varying acoustic impedance at the nozzle's outlets. This impedance shifts the mode from the computed value and, added to transitory effects, it is enough

to give the LES curve the behavior shown on Fig. 7. Nevertheless, the StaHF code is able to retrieve the level of pressure achieve by the LES computation.

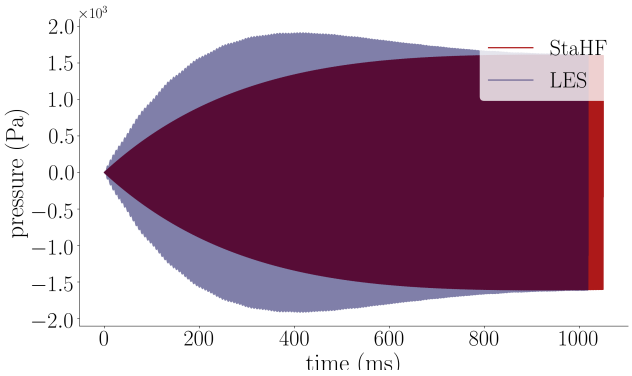

Figure 7: Pressure variation in the chamber (HFc1) for a 1T1L modulation, from LES (blue) and StaHF (red)

6. SUMMARY AND CONCLUSION

The low order modeling reviewed here is based on a modal expansion of the pressure variations over the eigenmode's base. Combustion of flame response under transverse solicitations models are given. Driving and damping terms enable the retrieval of experimental and numerical results, showing the approach's capabilities to be used as a prediction tool for thermo-acoustic instabilities in the liquid rocket engine framework. In the particular case of the configuration proposed by [3], the StaHF stability computation shows results fitting the theoretical results up to a relative error of 0.1%. Although some simplifying hypotheses have been made, the tool's robustness and capabilities are demonstrated and extended. Compared to an LES computation, an application to a real case is encouraging; so far, the limitations that have arisen seem to come from adequately modeling physical processes and implementing them in the framework rather than the framework itself.

It is necessary to enhance the modeling of the damping phenomena to limit the use of poorly mastered parameters. A modeling of the acoustic damping in cavities needs to be performed to account for the associated processes, such as boundary conditions, thermal and viscous losses or turbulence-acoustic coupling. First work on the modeling of impedance at the nozzle outlet though a dedicated source term show promising results, close to the impedance analysis made by [23]. Then, a comprehensive approach of the damping due to viscous and thermal losses near the walls is made by [29], and will make it possible to refine the damping estimation coefficients.

7. ACKNOWLEDGMENT

This work is part of an ongoing PhD thesis at EM2C laboratory, cofounded by CNES, the French National Space Agency and ArianeGroup. A part of this work was performed using HPC resources from the mesocentre computing center of Ecole CentraleSupélec and Ecole Normale Supérieure Paris-Saclay supported by CNRS and Région Ile-de-France. The LES computation mentioned in the last section were carried out by D. Marchal, Ph.D student at EM2C laboratory.

8. REFERENCES

[1] L. Crocco and S.-I. Cheng. Theory of combustion instability in liquid propellant rocket motors. *Butterworths Scientific Publications*, 1956.

[2] D.T. Harrje and F.H. Reardon. Liquid propellant rocket combustion instability. *Technical Report SP-194, NASA*, 1972.

[3] K. R. McManus, T. Poinsot, and S. M. Candel. A review of active control of combustion instabilities. *Progress in Energy and Combustion Science*, 19(1):1–29, 1993.

[4] J.C. Oefelein and Y. Vigor. Comprehensive review of liquid-propellant combustion instabilities in f-1 engines. *Journal of Propulsion and Power*, 9(5):657–677, 1993.

[5] G. Singla, P. Scouflaire, C. Rolon, and S. Candel. Transcritical oxygen/transcritical or supercritical methane combustion. *Proceedings of the Combustion Institute*, 30 II(2):2921–2928, 2005.

[6] Y. Méry, L. Hakim, P. Scouflaire, L. Vingert, S. Ducruix, and S. Candel. Experimental investigation of cryogenic flame dynamics under transverse acoustic modulations. *Comptes Rendus - Mecanique*, 341(1-2):100–109, 2013.

[7] J.S. Hardi and M. Oschwald. Cryogenic oxygen jet response to transverse acoustic excitation with the first transverse and the first combined longitudinal-transverse modes. *Progress in Propulsion Physics*, 8:75–94, 2016.

[8] A. Ficuciello, F. Baillot, J. B. Blaisot, C. Richard, and M. Théron. Acoustic response of an injection system to high-frequency transverse acoustic fields. *International Journal of Spray and Combustion Dynamics*, 9(4):217–229, 2017.

[9] N. Fdida, J. Hardi, H. Kawashima, B. Knapp, M. Oschwald, and A. Ristori. Flame response to high-frequency oscillations in a cryogenic oxygen/hydrogen rocket combustor. *Progress in Propulsion Physics*, (11):407–424, 2019.

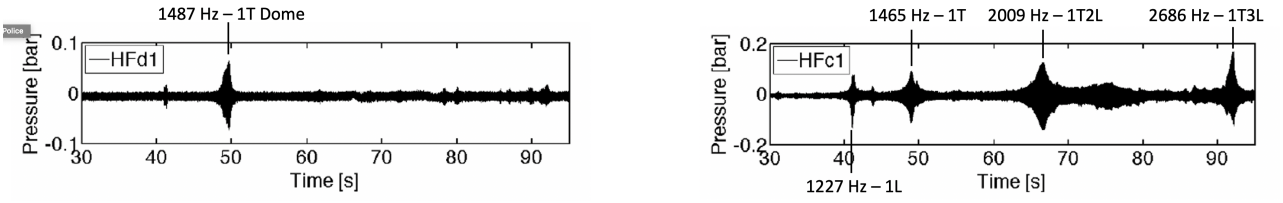

(a) (b)

Figure 8: Pressure response in the dome (a) and the chamber (b) from a frequency ramp 0 to 3000 Hz, [27]

(a) (b)

Figure 9: Pressure response in the dome (a) and the chamber (b) from a frequency ramp 0 to 3000 Hz, from StaHF

[10] W. Armbruster, J.S. Hardi, Suslov D., and M. Oschwald. Experimental investigation of self-excited combustion instabilities with injection coupling in a cryogenic rocket combustor. *Acta Astronautica*, 151:655 – 667, 2018.

[11] R Nez, D Marchal, T Schmitt, P Scouflaire, S Candel, and S Ducruix. Experimental and numerical characterizations of acoustic damping rates in a coupled-cavity configuration. *8th European Conference for Aeronautics and Aerospace Sciences (EUCASS)*, 2019.

[12] S. Klein, M. Börner, J.S. Hardi, D. Suslov, and M. Oschwald. Injector-coupled thermoacoustic instabilities in an experimental LOX-methane rocket combustor during start-up. *CEAS Space Journal*, 2020.

[13] L. Hakim, A. Ruiz, T. Schmitt, M. Boileau, G. Staffelbach, S. Ducruix, B. Cuenot, and S. Candel. Large eddy simulations of multiple transcritical coaxial flames submitted to a high-frequency transverse acoustic modulation. *Proceedings of the Combustion Institute*, 35(2):1461–1468, 2015.

[14] Y. Morii, S. Beinke, J.S. Hardi, T. Shimizu, H. Kawashima, and M. Oschwald. Dense core response to forced acoustic fields in oxygen-hydrogen rocket flames. *Propulsion and Power Research*, 9(3):197–215, 2020.

[15] A. Urbano, Q. Douasbin, and L. Selle. Analysis of coaxial-flame response during transverse combustion instability. *7th European Conference for Aeronautics and Aerospace Science (EUCASS)*, 2017.

[16] J. Xiong, H. Morgan, J. Krieg, F. Liu, and W.A. Sirignano. Nonlinear combustion instability in a multi-injector rocket engine. *AIAA Journal*, 58(1):219–235, 2020.

[17] C. Laurent, M. Bauerheim, T. Poinsot, and F. Nicoud. A novel modal expansion method for low-order modeling of thermoacoustic instabilities in complex geometries. *Combustion and Flame*, 206:334–348, 2019.

[18] J. Li, D. Yang, C. Luzzato, and A.S. Morgans. Open Source Combustion Instability Low Order Simulator (OSCILOS-Long) Technical report Open Source Combustion Instability Low Order Simulator. *Imperial College, London, UK*, 2015.

[19] B.T. Zinn and M.E. Lores. Application of the Galerkin Method in the Solution of Non-linear Axial Combustion Instability Problems in Liquid Rockets. *Combustion Science and Technology*, 4(1):269–278, 1971.

[20] M. Gonzalez-Flesca, P. Scouflaire, T. Schmitt, S. Ducruix, S. Candel, and Y. Méry. Reduced order modeling approach to combustion instabilities of liquid rocket engines. *AIAA Journal*, 56(12):4845–4857, 2018.

[21] F.E.C. Culick. Nonlinear behavior of acoustic waves in combustion chambers. *Acta Astronautica*, 3(9-10):735–757, 1976.

[22] F.E.C. Culick. Unsteady motions in combustion chambers for propulsion systems. *NATO Research and Technonoly Organization*, (AC/323 (AVT-039) TP/10), 2006.

[23] G. Ghirardo, F. Boudy, and M. R. Bothien. Amplitude statistics prediction in thermoacoustics. *Journal of Fluid Mechanics*, 844:216–246, 2018.

[24] F. Nicoud, L. Benoit, C. Sensiau, and T. Poinsot. Acoustic modes in combustors with complex impedances and multidimensional active flames. *AIAA Journal*, 45(2):426–441, 2007.

[25] T. Poinsot and D. Veynante. Theoretical and numerical combustion. *Edwards*, 2nd edition, 2005.

[26] Y. Mery. Mécanismes d'instabilités de combustion haute-fréquence et application aux moteurs-fusées. *Ph.D. thesis, Ecole Centrale Paris*, 2010.

[27] M. Gonzalez-Flesca. Simulation, experimentation and modeling contributions to the analysis of high frequency combustion instabilities in liquid propellant rocket engines. *PhD Thesis, CentraleSupélec, Université Paris-Saclay*, 2016.

[28] L. Hakim. Dynamics of transcritical coaxial flames in high-frequency transverse acoustic fields: application to liquid rocket engine instabilities. *Ph.D. thesis, Ecole Centrale Paris*, 2013.

[29] G. Searby, A. Nicole, M. Habiballah, and E. Laroche. Prediction of the efficiency of acoustic damping cavities. *Journal of Propulsion and Power*, 24(3):516–523, 2008.